Eur. Phys. J. C 8, 59–66 (1999)
DOI 10.1007/s100529901103

THE EUROPEAN PHYSICAL JOURNAL C

First observation of Σ^--e^- elastic scattering in the hyperon beam experiment WA89 at CERN

The WA89 Collaboration

M.I. Adamovich[8], Yu.A. Alexandrov[8], D. Barberis[3], M. Beck[5], C. Bérat[4], W. Beusch[2], M. Boss[6], S. Brons[5,a], W. Brückner[5], M. Buénerd[4], C. Busch[6], C. Büscher[5], F. Charignon[4], J. Chauvin[4], E.A. Chudakov[6,b], U. Dersch[5], F. Dropmann[5], J. Engelfried[6,c], F. Faller[6,d], A. Fournier[4], S.G. Gerassimov[5,8,e], M. Godbersen[5], P. Grafström[2], Th. Haller[5], M. Heidrich[5], E. Hubbard[5], R.B. Hurst[3], K. Königsmann[5,f], I. Konorov[5,8], N. Keller[6], K. Martens[6,g], Ph. Martin[4], S. Masciocchi[5,h], R. Michaels[5,b], U. Müller[7], H. Neeb[5], D. Newbold[1], C. Newsom[i], S. Paul[5,e], J. Pochodzalla[5], I. Potashnikova[5], B. Povh[5], R.D. Ransome[j], Z. Ren[5], M. Rey-Campagnolle[4,k], G. Rosner[7], L. Rossi[3], H. Rudolph[7], C. Scheel[l], L. Schmitt[7,e], H.-W. Siebert[6], A. Simon[6,f], V.J. Smith[1,m], O. Thilmann[6], A. Trombini[5], E. Vesin[4], B. Volkemer[7], K. Vorwalter[5], Th. Walcher[7], G. Wälder[6], R. Werding[5], E. Wittmann[5], M.V. Zavertyaev[8]

[1] University of Bristol, Bristol, UK
[2] CERN, CH-1211 Genève 23, Switzerland
[3] Genoa University/INFN, Dipartimento di Fisica, I-16146 Genova, Italy
[4] Grenoble ISN, F-38026 Grenoble, France
[5] Heidelberg Max-Planck-Institut für Kernphysik, Postfach 103980, D-69029 Heidelberg, Germany
[6] Universität Heidelberg, Physikal. Institut, D-69120 Heidelberg Germany[n]
[7] Universität Mainz, Institut für Kernphysik, D-55099 Mainz, Germany[n]
[8] Moscow Lebedev Physics Institute, 117924 Moscow, Russia

Received: 23 October 1998 / Published online: 1 March 1999

Abstract. We have investigated the elastic scattering of high energy Σ^- off electrons from carbon and copper targets using the CERN hyperon beam. Scattering events are identified using a maximum likelihood technique exploring the kinematical relations of the scattered particles. The observed Q^2–distribution of these events suggests a mean square charge radius of the Σ^- of $< r_{ch}^2 > (\Sigma^-) = 0.91 \pm 0.32(stat.) \pm 0.4$ (syst.) fm^2. This constitutes the first measurement of $< r_{ch}^2 > (\Sigma^-)$ and demonstrates the possibility to also measure the charge radii of other hyperons.

1 Introduction

Hadrons are extended objects which can be described by a number of static properties such as the mass, magnetic moment, strong interaction radius, and charge radius. Although the basic structure of hadrons is believed to be described by quantum chromodynamics (QCD), concrete calculations of these quantities remain problematic. Additionally, many of these fundamental properties are well known only for nucleons. Some, in particular the electric mean squared charge radius $< r_{ch}^2 >$, are measured only for the nucleons [1–4], the π^- [5], and the K^- [6]. In this paper we discuss the first measurement of $< r_{ch}^2 >$ for a strange baryon, the Σ^-.

Since exact calculations based on QCD are not yet possible, calculations of $< r_{ch}^2 >$ of the Σ^- have been carried out in the context of a variety of models which attempt to approximate QCD in the nonperturbative region [7–12]. The primary non-perturbative method is lattice QCD [13–15]. Although tremendous progress has been

[a] Now at TRIUMF, Vancouver, B.C., Canada V6T 2A3
[b] Now at Thomas Jefferson Lab, Newport News, VA 23606, USA
[c] Now at Institudo de Fisica, Universidad San Luis Potosi, S.L.P. 78240, Mexico
[d] Now at Fraunhofer Institut für Solarenergiesysteme,D-79100 Freiburg, Germany
[e] Now at Technische Universität München, Garching, Germany
[f] Now at Fakultät für Physik, Universität Freiburg, Germany
[g] Now at Kamioka Observatory, Institute for Cosmic Ray Research, University of Tokyo,Ja
[h] Now at Max-Planck-Institut für Physik, München, Germany
[i] University of Iowa, Iowa City, IA 52242, USA
[j] Rutgers University, Piscataway, NJ 08854, USA
[k] permanent address: CERN, CH-1211 Genève 23, Switzerland
[l] NIKHEF,1009 DB Amsterdam, The Netherlands
[m] supported by the UK PPARC
[n] supported by the Bundesministerium für Bildung, Wissenschaft, Forschung und Technologie, Germany, under contract numbers 05 5HD15I, 06 HD524I and 06 MZ5265

made in the past few years, lattice QCD calculations remain difficult and inexact, especially when light quarks are involved. The predicted radii vary considerably - from as small as 0.50 fm^2 in the MIT bag model, to 1.2 fm^2 in a recent Skyrme model based calculation. However, within each of these models, the radius is predicted to be within about 20% of that predicted for the proton, which has a measured value of about $\langle r^2_{ch}\rangle$=0.73 fm^2. The predictions of a number of models are summarized in Table 1.

The scattering of an electron with mass m and a spin 1/2 particle of mass M can be approximated by the relation ($\hbar$= c = 1) [16]

$$\frac{d\sigma}{dQ^2} = \frac{4\pi\alpha^2}{Q^4}\left(1-\frac{Q^2}{Q^2_{max}}\right)F^2(Q^2) \qquad (1)$$

where deviations from the exact value are of the order $m^2/(s-M^2)$. For $m \ll M$ the squared form factor can be written as

$$F^2(Q^2) = \frac{G_E^2 + \frac{Q^2}{4M^2}G_M^2}{1+\frac{Q^2}{4M^2}} + \frac{Q^4}{2(4m^2E^2-(2mE+M^2)Q^2)}G_M^2. \qquad (2)$$

Here, Q^2 is the squared momentum transfer and $G_E(Q^2)$ and $G_M(Q^2)$ are the electric and magnetic form factors, respectively. These form factors are normalised to $G_E(0)$ = -1 and $G_M(0) = \kappa - 1$, κ being the anomalous magnetic moment (equal to -0.48 in units of μ_Σ where $\mu_\Sigma = e\hbar/(2M)$ denotes the Dirac magnetic moment of the Σ^-). The mean squared charge radius is defined by the relation

$$< r^2_{ch} >= -6G_E(0)\left.\frac{dG_E}{dQ^2}\right|_{Q^2=0}. \qquad (3)$$

Expanding the squared form factor F^2 and using the above normalisations we can write

$$\frac{d\sigma}{dQ^2} = \frac{4\pi\alpha^2}{Q^4}\left(1-\frac{Q^2}{Q^2_{max}}\right)\cdot\left(1-\frac{1}{3}< r^2_{ch} > Q^2 + \frac{\left[(\kappa-1)^2-1\right]}{4M^2}Q^2 + O(Q^4)\right). \qquad (4)$$

The measurement of the radius does not rely on the absolute magnitude of the cross section. Instead, a fit of equation (4) to the *shape* of the measured Q^2 distribution will provide the information on $< r^2_{ch} >$. Since the kinematics of an elastic scattering event is constrained by conservation of momentum and energy, the determination of Q^2 does not in principle demand complete kinematic information on all participating particles. However, detector resolution and the problem of radiative effects render the extraction of the cross section distribution more difficult. The resulting uncertainties will be discussed in the analysis section.

2 The experiment

The measurement described here is part of CERN experiment WA89, a general purpose apparatus with the primary goal of studying charmed particles and their decays. Σ^- scattering events are extracted from a low multiplicity trigger running simultaneously with the main experiment trigger.

The experiment makes use of a negatively charged secondary beam produced in forward direction by a 450 GeV/c proton beam impinging on a 40 cm long beryllium target. The primary proton beam is extracted from the SPS in a 2.5 s "spill" every cycle of 14.7 s. Typically a spill contains 5×10^{10} protons. Secondary particles with momenta of 330 $\pm$ 15 GeV/c are selected by means of a 14 m long magnetic channel defined by tungsten collimators [17]. At the target of the experiment the secondary beam has a total intensity of 7×10^5/spill and is composed of π^- and Σ^- in the ratio of 2.3:1. Other particles, primarily $\Xi^-$and K^-, constitute less than 3% of the beam.

The momentum of each beam particle is measured by a scintillating fiber hodoscope placed between the last two magnets of the channel, along with two sets of silicon detectors at the end of the channel. The fiber hodoscope is made from four planes of rectangular fibers (1×0.5 mm^2). Always two planes, staggered by half a fiber width (0.25 mm), are read out by one multi-anode photo multiplier. The track finding requires hits in at least two planes and a good extrapolation of the track to the hyperon production target. An efficiency of about 90% is obtained. The resulting momentum resolution is approximately 1%.

The detector set-up is shown in the upper part of Fig. 1. The main components are

- the target region (see lower part of Fig. 1 for a more detailed graph) composed of trigger scintillators, a transition radiation detector (TRD), high resolution microstrip detectors, and microstrip gas chambers (MSGCs),
- the decay region which is equipped with several planes of drift chambers and multi-wire proportional chambers (MWPCs),
- the Ω-spectrometer,
- a ring imaging Cherenkov detector and
- electromagnetic and hadronic calorimetry.

The beam is defined by two 3×3 cm^2, 3 mm thick scintillators upstream of the targets. A TRD consisting of 10 radiator-detector pairs has been placed between the two scintillators for beam particle identification. The TRD has a π^- rejection efficiency of about 90% at the trigger level [18]. The incoming beam particle direction is reconstructed by means of 7 silicon microstrip planes with 25/50 μm pitch [20]. An angular precision of about 15 μrad is achieved.

One 3.6 g/cm^2 thick copper block followed by three 0.72 g/cm^2 thick pressed diamond plates (density 3.25 g/cm^3), each separated by 2 cm and placed in a box flushed with helium serve as scattering targets. Located immediately behind the targets are 12 planes of silicon detectors, two 5×5 cm^2 scintillators with thicknesses of 3 mm and 4mm, respectively, and again 11 planes of silicon detectors. The first 16 silicon planes have a read-out pitch of 25 μm, the remaining seven have a 50 μm pitch. The

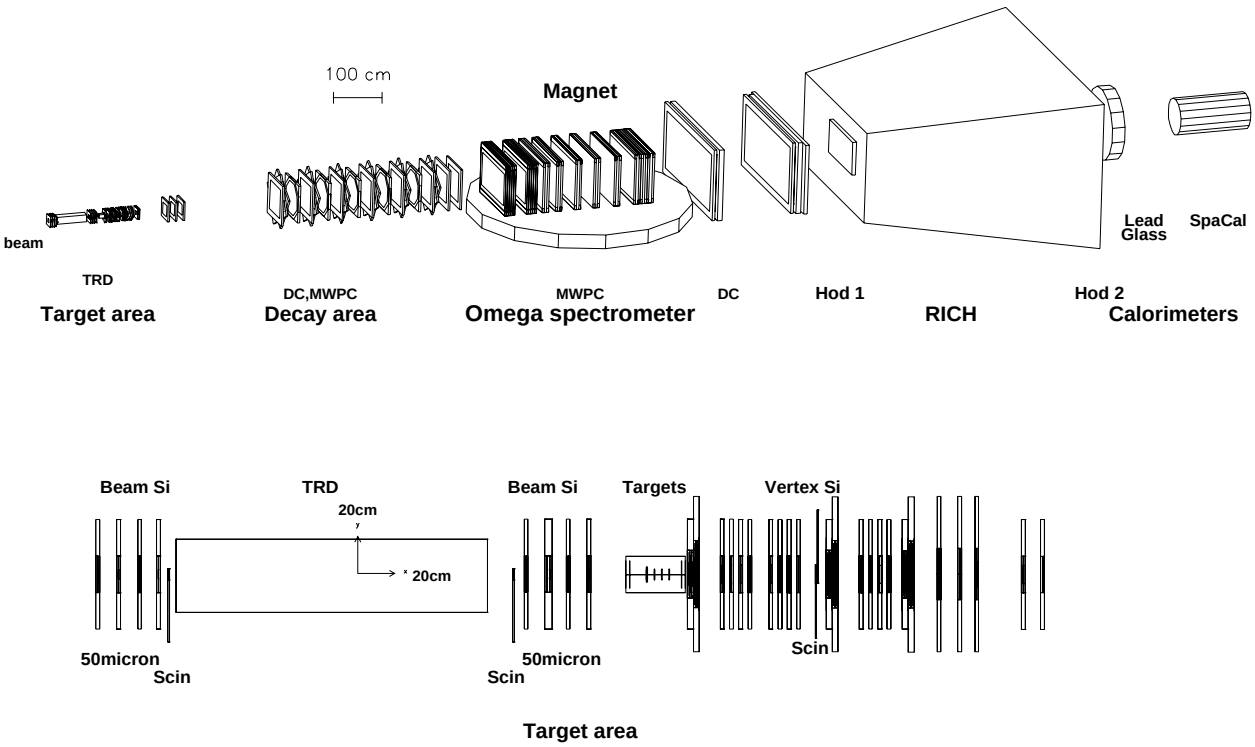

Fig. 1. Setup of experiment WA89. The lower part shows an expanded view of the target area

Table 1. Measured $\langle r^2_{ch} \rangle$ in fm^2 of various hadrons along with some theoretical predictions for p, n, and Σ^-

	Experiment	Soliton [7]	Skyrme [8]	non-relat. quark [12]	Skyrme [9]	Cloudy Bag [11]
p	0.74 ± 0.02 [1]	0.78	1.20	0.67	0.775	0.714
	0.67 ± 0.02 [2]					
	0.79 ± 0.03 [3]					
n	-0.11 ± 0.03 [4]	-0.09	-0.15		-0.308	-0.121
Σ^-	0.91 ± 0.32 ±0.4	0.75	1.21	0.55	0.751	0.582
π^-	0.439 ± 0.008 [5]					
K^-	0.34 ± 0.02 [6]					

two scintillators play a central role for the event trigger (see below).

The target region is followed by a 10 m long "decay zone", filled with 6 stacks of drift chambers (3 projections each) and MWPCs for the central part (4 projections each). These are used primarily for reconstruction of Λ and K^0 decays.

A magnetic spectrometer based on the large gap superconducting OMEGA dipole magnet (7.2 Tm) provides the charge and momentum information of the outgoing particles. The detectors consist of 45 planes of MWPCs between the pole faces of the magnet and two sets of drift chambers with four planes each downstream of the magnet. Four additional MWPC planes placed close to these drift chambers are used in the trigger for track multiplicity decisions. A momentum resolution of about $10^{-4} \times p^2/$ GeV$^2/c^2$ is achieved.

A large ring imaging Cherenkov detector (RICH) is employed to identify high momentum particles [21]. The geometrical acceptance of this detector is limited to particles above ≈ 15 GeV/c. The detector allows π/K/p separation in the momentum range of 20 to 80/140 GeV/c. π/electron separation is possible only in a very small momentum interval up to about 20 GeV/c.

An electromagnetic calorimeter made out of 640 lead glass blocks [19] is placed downstream of the RICH. Its main purpose is the detection of γ from radiative or π^0 decays and its size of 3.2 m^2 enables the detection of electrons with momenta above 25 GeV/c.

Located behind the lead glass array is a lead scintillating fiber calorimeter of the spaghetti type [22]. It has an energy resolution of about $(30\sqrt{E} + 2.5)\%$ and a position resolution of $(3.14/\sqrt{E}+0.24)$cm, where E is given in GeV. This calorimeter plays an important role for the

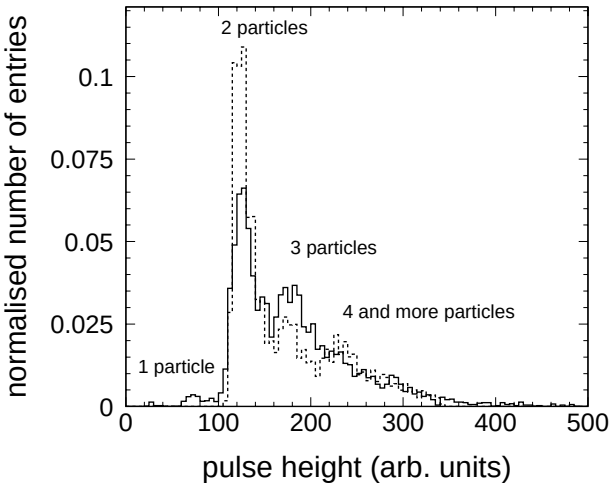

Fig. 2. Normalized pulse height distribution in one of the two multiplicity trigger counters. Solid line: data; dashed line: Monte Carlo results. Multiplicities below 3 were partially cut by the trigger. In the final analysis only events with a pulse height $\leq$155 were used

detection of neutrons from charm or Σ^--decays. In addition, a scintillating tile hodoscope covering the front face allows to tag showers generated by charged hadrons [23].

The main trigger of the experiment is set up to enrich the data sample with events containing charmed hadrons. Downstream of the 12th silicon plane in the vertex detector, two thin scintillator counters (3 and 4mm thickness) are used to select events with large track multiplicities (n_{ch} $\geq$5). The collection of events containing scattered target electrons is realized by an additional trigger with a threshold corresponding to two charged particles in each scintillator. Because of the high rate of this trigger it is then pre-scaled by a factor 2. Due to an undetected base line drift in one of the counters during the running phase one counter selected only events with energy depositions characteristic for more than 2 tracks for a large fraction of the running time. Unfortunately this leads to a rejection of a considerable part of the genuine 2 track scattering events. However, because of the large Landau tail of the energy loss distribution also a considerable fraction of the 2 prong events give a sufficiently large signal in both detectors to pass the trigger decision. This can be seen by the solid histogram in Fig. 2 which shows the pulse height distribution of the scintillator without the base line shift.

These conditions constitute the first trigger level and are a compromise between the constraints on the trigger rate given by the main experimental program of WA89 and the requirements for the detection of Σ^-e^- scattering events. At the second level, we use the information from the beam TRD to reduce the number of π-induced reactions by $\approx$ 95% while keeping 85% of the Σ^- .

The present analysis is based on about 3×10^8 interactions, recorded during our 1994 beam time. Approximately 25% of these events are due to low multiplicity events.

3 Analysis of Σ^--e scattering

3.1 Event preselection

The first step of the analysis is to isolate those events in which exactly two negative particles are seen in the Ω spectrometer. The simple topology of the events with only two outgoing negatively charged particles allows us to apply a straightforward reconstruction algorithm. The Σ^--e scattering events can be subdivided into two main categories: events where the Σ^- passes through the spectrometer magnet without decaying and those in which the Σ^- decays within the apparatus to $n\pi^-$(branching ratio for this mode : 99.85%). The distance from the silicon strip detectors to the Ω-spectrometer is about 10 m and is, therefore, comparable to the mean decay length $\beta c\tau\gamma \approx$ 12 m for a Σ^- at 330 GeV/c. Thus about half of the Σ^- decay before reaching the spectrometer. In either case, the final state consists of two negatively charged particles plus one neutron if the Σ^- decays.

Generally, straight tracks in the vertex detector and the decay region are independently reconstructed and then connected to tracks found in the spectrometer. Σ^- hyperons which decay before the Ω-magnet are reconstructed from the $n\pi^-$ final state by using the energy of the decay neutron determined with help of the hadronic calorimeter. Such neutrons are then combined with a track that started only in the decay region. The intersection of such tracks with a track segment in the vertex detector is taken as the Σ^- decay point. The invariant mass of such $n\pi^-$ combinations is then checked to be compatible with the Σ^- mass. For this reconstruction an accurate momentum measurement for the π^- from the Σ^- decay is mandatory. Therefore, Σ^- which decayed within the Ω-spectrometer magnet can not be used in the analysis. Finally, the Σ^- four momentum was refitted with the constraint for the $n\pi^-$ to correspond to the nominal Σ^- mass. Thus a similar momentum resolution was obtained as for Σ^- passing the spectrometer.

This first part of the analysis reduces the number of analysed events from over 300 million to about 4 million. All further analysis is based on this selected sample.

3.2 Further event selection cuts

In order to determine the position of the scattering vertex we perform a 3-prong vertex fit with the incoming beam track and the two outgoing tracks. We require the χ^2 of the vertex fit to be less than 2.5 in order to reject events with poorly reconstructed vertices. A good vertex resolution is necessary, since the amount of material crossed by the electron determines the bremsstrahlung losses and is, therefore, an important input to calculate the probability distribution of the electron momentum event-by-event (see below). Figure 3.a shows the angular correlation between the scattered Σ^- and the electron after applying this cut. The number of remaining events is given in the figure. The lower and upper lines in this plot mark the expected correlations for an elastic scattering of a 330 GeV/c Σ^-

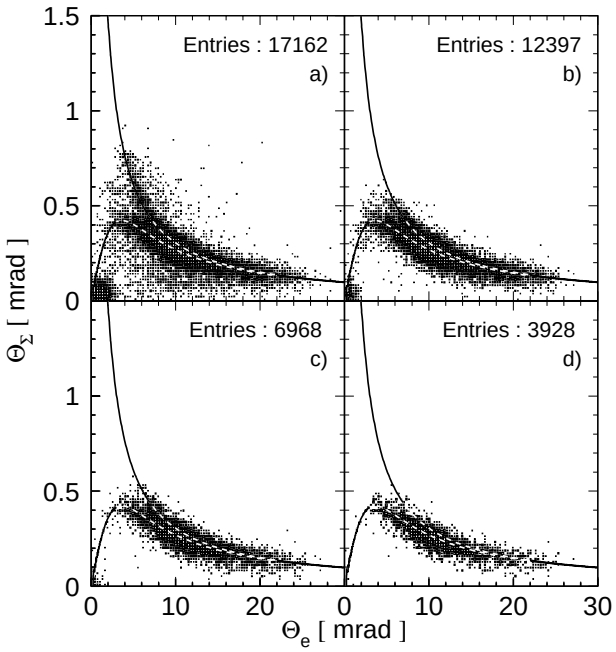

Fig. 3. Correlation between the Σ^- and e^- scattering angles. a: data sample after vertex reconstruction. b: data sample after kinematical fit. c: data sample with cut on pulse height in multiplicity counter and d: after applying offline beam particle identification. The lines mark the relation expected for elastic Σ^-e and π^-e scattering. In the final fit to determine the radius a Q^2 between 0.01 and 0.05 GeV^2/c^2 was required (see Sect. 3.4) which corresponds to electron scattering angles between approximately 2-9 mrad

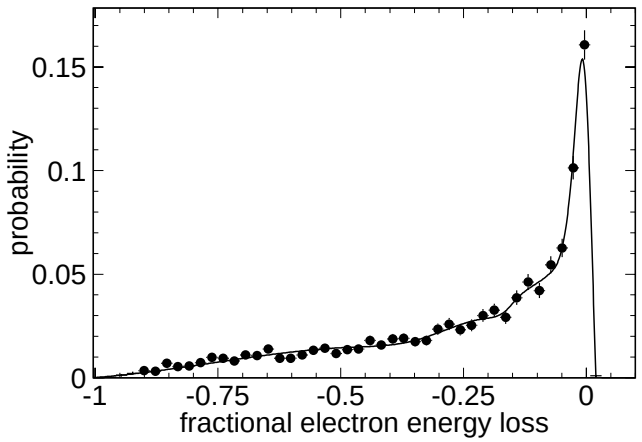

Fig. 4. Distribution of the fractional energy loss of the electron used in the likelihood fit of the momentum transfer Q^2. The solid curve corresponds to a spline parametrisation of the curve used in the Q^2 fit. The integral of the histogram is normalised to 1.0 and can therefore be interpreted as a probability distribution

and π^-, respectively. Contributions from either beam particle are clearly visible in the data. Therefore, a number of additional event selection criteria have to be employed to clean up the data sample.

For the evaluation of the four momentum transfer of the beam particle to the electron from the measured quantities p_B (beam momentum), Θ_e (electron scattering angle), Θ_Σ (Σ^- scattering angle), p_e (momentum of scattered electron) and p_Σ (momentum of scattered Σ^-), several possibilities exist which allow to check the kinematic relations event-by-event. To exploit all measurement information we calculate the likelihood

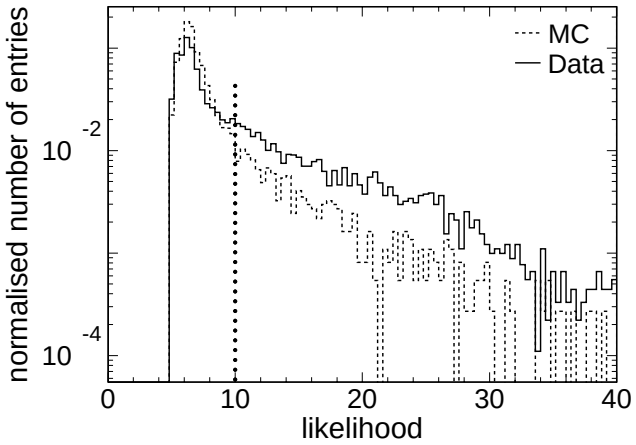

Fig. 5. Distribution of likelihood goodness $\mathcal{L}_{min}$ for Data (solid line) and Monte-Carlo (dashed line). The vertical line indicates the applied cut. Both histograms were normalised to 1

$$\mathcal{L}(Q^2) = P_1(p_B)P_2(\Theta_e)P_3(\Theta_\Sigma)P_4(p_e)P_5(p_\Sigma) \qquad (5)$$

and maximize it to find the best estimates for Q^2 and the beam momentum p_B^0. Here, $P_i(X_i)$ is the probability of measuring the quantity X_i at given values of Q^2 and p_B^0. Shape and width of the probability functions P_i are defined by the detection resolution and are derived on an event by event basis from the covariance matrices of the track parameters. Except for $P_4(p_e)$ these functions are Gaussian–distributed. The shape of $P_4(p_e)$ follows a Bethe-Heitler distribution [24], since the error on p_e is dominated by Bremsstrahlung losses in the targets and detectors. An example of the probability distribution $P_4(p_e)$ for an interaction in the copper target obtained in the GEANT detector simulation is shown in Fig. 4. Since the electron energy loss depends on the material traversed by the electron, the energy loss probability was parametrised in dependence of the position of the interaction vertex.

The likelihood Q^2 fit checks the complete kinematics of an event and assigns a value $\mathcal{L}_{min} = min(-\log\mathcal{L})$. Smaller values signal better agreement with the topology of a two-body elastic scattering event. The goodness of this likelihood fit is used as a cut criterion. In the Monte–Carlo–simulation in 86% of the events we obtain $\mathcal{L}_{min}$ values below 10. In contrast, $\approx 40\%$ of the measured preselected data assume larger values (Fig. 5). Applying the condition $\mathcal{L}_{min} < 10$ and the χ^2 cut mentioned above considerably cleans up the scattering angle spectra, as can be seen in Fig. 3.b. In particular large Q^2 π^-e$^-$ scattering events are rejected by this constraint.

This figure still exhibits a sizable yield at large Q^2 (small scattering angles) which is caused by inelastic interactions of higher multiplicities, where one or more low

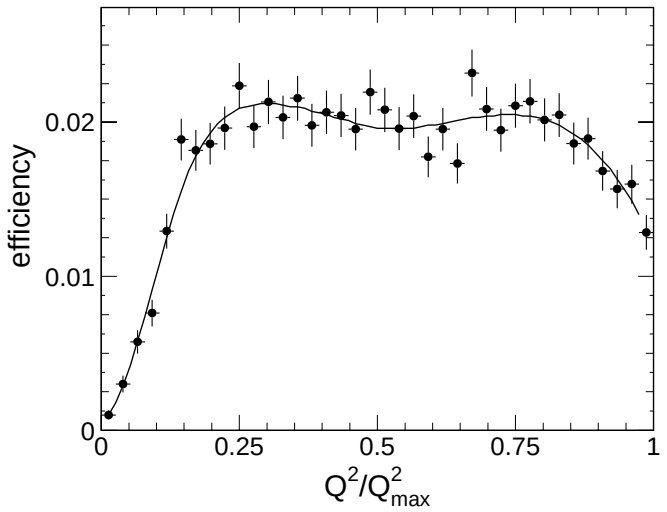

Fig. 6. Detection and reconstruction efficiency for Σ^--e$^-$scattering events predicted by Monte Carlo simulations and plotted as a function of Q^2/Q^2_{max}. The curve is a cubic spline fit through the data points

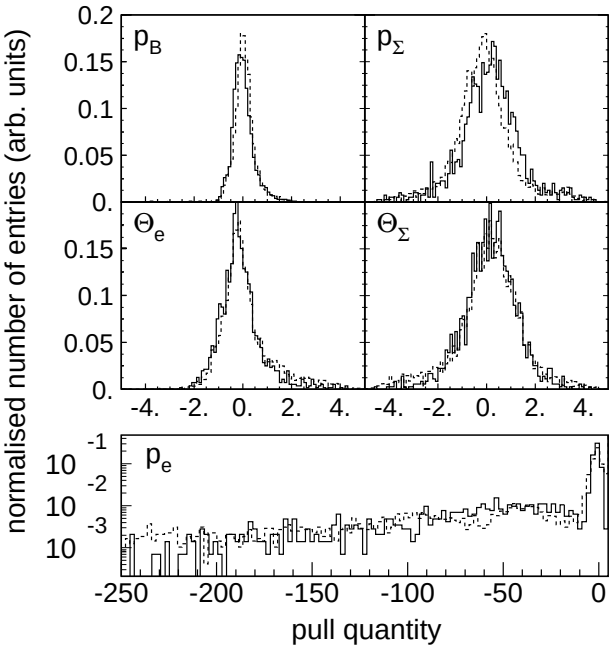

Fig. 7. Pull quantities $(x_{measument} - x_{fit})/\sigma_x$ from the likelihood fit of the momentum transfer Q^2. Here, x denotes the kinematic quantity indicated in the figure. Results for experimental data and for Monte Carlo events are given by the solid and dashed histograms, respectively

momentum tracks are not reconstructed in the detector. In order to reject this kind of events we make use of the pulse height information recorded by the trigger scintillators. The solid histogram in Fig. 2 shows the pulse height spectrum of the scintillator without the base line shift discussed above for preselected events. A clear signal can be seen from events with 2, 3 and more tracks traversing this detector. For comparison the shape of the detector response obtained in a detector simulation for pure Σ^--e scattering event is shown by the dashed line. Good agreement is obtained between Monte Carlo and data.

Fig. 3.c shows the correlation of the scattering angles after a pulse height cut of $\leq$155 (cf. Fig. 2) was applied. There still remains a visible contamination of π^- in the Σ^- events, where the scattered Σ^- is not identified by its decay. This is because both event types show the same kinematics at low Q^2. To suppress the remaining π^- contamination, we exploit the pulse height information from the TRD [17,18] by means of a likelihood analysis. Figure 3.d displays the correlation of the projectile and electron scattering angles after requiring that the beam particle was identified offline as a Σ^- .

3.3 Detector simulation

To determine the apparatus acceptance and the event reconstruction efficiency a full Monte Carlo simulation was carried out in the GEANT 3.21 framework [25]. Beam particles were generated with the measured momentum distribution and induced a Σ^--e$^-$scattering event. A flat spectrum in Q^2 was chosen for the scattering kinematics in the Monte Carlo to measure the efficiency over the full phase space. Subsequently the generated events were passed through the same reconstruction and analysis process as the real data.

The detection efficiency as function of Q^2/Q^2_{max} for scattering events surviving preselection and all analysis cuts described above is shown in Fig. 6. Here, Q^2_{max} denotes the maximum possible momentum transfer for a given beam momentum. The efficiency was parametrised in the variable Q^2/Q^2_{max} to reduce the influence of the beam momentum distribution. For Σ^--e scattering at an average beam momentum of 330 GeV/c $Q^2_{max} \approx 0.065$ GeV$^2/c^2$.

Only electrons with momenta greater than 6 GeV/c can be reconstructed with high efficiency in the Ω-spectrometer. For Σ^--e$^-$elastic scattering this value corresponds to a maximum electron angle of $\approx$12 mrad and constrains the Q^2 of detectable events to a minimum value of about 0.006 GeV$^2/c^2$. In addition, the requirement for the electron to pass the trigger hodoscope increases the minimum electron momentum to about 10-12 GeV/c. This effect is the main reason for the efficiency drop at $Q^2/Q^2_{max} \approx 0.2$.

Towards high Q^2/Q^2_{max} the opening angle between the scattered Σ^- and the electron is decreasing. Because of the finite double track resolution of the detectors upstream of the Ω-magnet, the efficiency drops again at high Q^2/Q^2_{max}.

The quality of the Q^2–determination via the likelihood method can be judged on the basis of the pull quantities, calculated from the difference of the fitted and the measured parameters relative to their errors. These pulls obtained in Monte Carlo (dashed histograms) and real data (solid histograms) are displayed in Fig. 7. Very good agreement is obtained between the simulation and the data and show the expected – nearly Gaussian – shape for

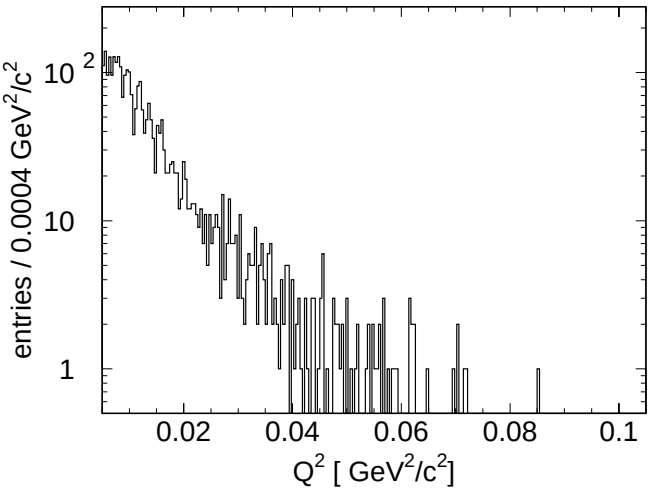

Fig. 8. Q^2 distribution of Σ^-e scattering events

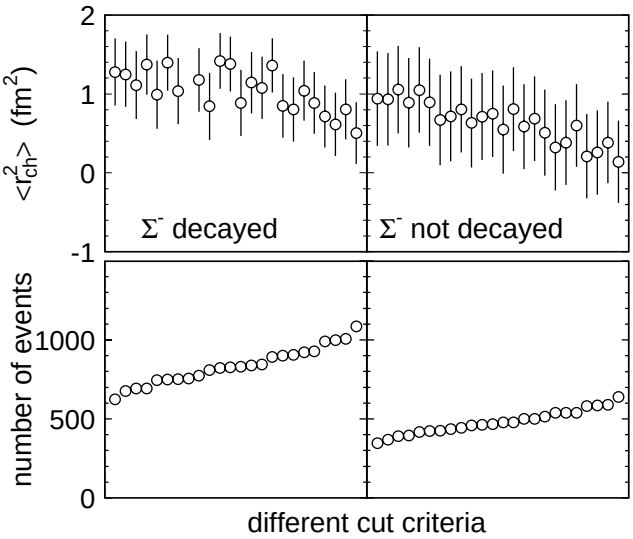

Fig. 9. $\langle r^2_{ch}\rangle$fit result for the sample with decayed (left) and undecayed (right) $\Sigma^-$and for different cut variations. The lower parts show the remaining sample size within the fitted Q^2 range from 0.01 to 0.05 GeV^2/c^2

$p_B, \Theta_e, \Theta_\Sigma$, and p_Σ, and a Bethe-Heitler type shape for p_e.

By a comparison of generated and measured momentum transfer in Monte Carlo events we determined the resolution in Q^2 obtained with this fit method. The distribution of $\Delta \mathrm{Q}^2/\mathrm{Q}^2$ shows two components: one from events where the electron has suffered no or small losses and one with large losses. The average resolution is 5.5 %.

3.4 Determination of the mean squared charge radii

The fact that the final data fall closely onto the correlation expected for Σ^-e scattering (see Fig. 3.d) together with the good agreement to the distributions expected from the Monte Carlo simulation is a clear evidence that these events correspond to elastic Σ^--e$^-$scattering. In order to extract the charge radius from our data we first corrected the measured Q^2 distribution shown in Fig. 8 for the finite efficiency (Fig. 6). Then, a charge radius for Σ^- can be determined by an unbinned maximum likelihood fit of the differential cross section given in 2. The detection efficiency shows a steep drop for small Q^2. As the actual shape of the acceptance and efficiency function in this range is difficult to evaluate we rejected events below $\mathrm{Q}^2 = 0.01$ GeV^2/c^2 . Due to the $1/\mathrm{Q}^4$–behavior of the cross section the bias caused by background events becomes increasingly important towards higher Q^2 . For this reason we also did not include events with $Q^2 > 0.05$ GeV^2/c^2 in the fit. The fit result for the Σ^- mean squared charge radius is $\langle r^2_{ch}\rangle(\Sigma^-) = 0.89 \pm 0.32$ (stat.) fm^2. This value represents the weighted mean from two separate fits to the samples with non-decayed and decayed Σ^- respectively.

Finally, the correction due the anomalous magnetic moment (see 4) amounts to 0.024 fm^2. Since this is small compared to our experimental error, uncertainties of this correction due to higher order effects have been neglected. We thus obtain our final value of $\langle r^2_{ch}\rangle(\Sigma^-) = 0.91 \pm 0.32$ (stat.) fm^2.

3.5 Study of systematic uncertainties

In order to study systematical effects we varied the applied selection criteria and the Q^2 range used in the fit. However, with the limited amount of scattering events detected a detailed study of systematic effects is rather difficult since some of the effects are masked by the large statistical fluctuations when different selection criteria or fit ranges are used in the analysis.

In the upper part of Fig. 9 we show the variation of the Σ^- radius fit results caused by variations of the cut on the likelihood, the cut on the vertex quality and the cut on the threshold of the multiplicity counter. Fit results for the samples of decayed Σ^- and non-decayed Σ^- are shown separately. The data points are ordered according to the number of events which passed the cuts (shown in the lower part of Fig. 9). Irrespective of the specific choice of the modified cut variable a general tendency towards smaller radii can be seen for more open cuts. This trend can be traced back to an increasing amount of background in the corresponding data sample and becomes even more prominent when the fit range is enlarged towards higher maximum Q^2. In general the results obtained from decayed Σ^- show slightly larger values for $\langle r^2_{ch}\rangle$ than the results obtained for non decayed Σ^-. In total the fit results vary between 0.15 fm^2 and 1.47 fm^2. We assign a systematical error of $(1.47 - 0.15)/\sqrt{12} \approx 0.4$ fm^2 to our measurement to account for the observed variations. Since this error is strongly related to the limited statistics at large Q^2, future experiments with improved statistics should be able to reduce also the systematical uncertainty significantly. Indeed, the SELEX collaboration has recently reported a Σ^- mean squared charge radius which is based on an event sample with more than a factor of 10 better statistics [26]. As a consequence, their preliminary result

of $\langle r^2_{ch}\rangle$ =0.6±0.08±0.08 fm^2 is significantly more accurate and lies within our quoted uncertainties.

4 Conclusion

In conclusion we have made the first observation of Σ^- - electron elastic scattering in inverse kinematics. From the scattering data a mean squared charge radius of

$$\langle r^2_{ch}\rangle(\Sigma^-) = 0.91 \pm 0.32(stat.) \pm 0.4(syst.)\mathrm{fm}^2$$

was obtained for the Σ^- . Unfortunately, a detailed comparison of this result with the data on the proton radius or a comparison with the radius difference between π and K is not possible on the basis of the present measurement. Nonetheless, this analysis clearly demonstrates the feasibility of more precise studies in the near future with improved statistics. At the same time the experimental method presented here demonstrates the possibility to extend such measurements to other hyperons using high-energy secondary beams.

Acknowledgements. We are pleased to thank J. Zimmer and the late Z. Kenesei for their assistance throughout construction and setup of the experiment as well as for their support during the running phase. We gratefully acknowledge the assistance of the Omega spectrometer group and the CERN SPS group.

References

1. G.G. Simon, Ch. Schmitt, F. Borkowski, and V. H. Walther, Nucl. Phys. A **333**, 381 (1980)
2. J.J. Murphy, Y.M. Shin and D.M. Skopik, Phys. Rev. C **9**, 2125 (1974)
3. Th. Udem et al., Phys. Rev. Lett. **79**, 2646 (1997)
4. S. Kopecky, P. Riehs, J. A. Harvey, N. W. Hill, Phys. Rev. Lett. **74**, 2427 (1995)
5. S. R. Amendolia, et al. , Nucl. Phys. B **277**, 168 (1986)
6. S. R. Amendolia, et al. , Phys. Lett. B **178**, 435 (1986)
7. H.C. Kim, A. Blotz, M. V. Polyakov, and K. Goeke, Phys. Rev. D **53**, 4013 (1996)
8. N. W. Park and H. Weizel, Nucl. Phys A **541**, 453 (1992)
9. J. Kunz, P. J. Mulders, and G. A. Miller, Phys. Lett. B **255**, 11 (1991)
10. T. DeGrand, R. L. Jaffe, K. Johnson, J. Kiskis, Phys. Rev. D **12**, 2060 (1975)
11. A. W. Thomas, S. Theberge, G. A. Miller, Phys. Rev. D **24**, 216 (1981)
12. B. Povh, Nucl. Phys. A **532**, 133c (1991); B. Povh and J. Hüfner, Phys. Lett. B **245**, 653 (1990)
13. M. Creutz, L. Jacobs, and C. Rebbi, Phys. Rep. **95**, 201 (1983)
14. D.B. Leinweber, R. M. Woloshyn, T. Draper, Phys. Rev. D **43**, 1659 (1991)
15. D.B. Leinweber and T. D. Cohen, Phys. Rev. D **47**, 2147 (1993)
16. G. Källén, *Elementary particle physics*, Addison-Wesley Publishing Company (1964)
17. Yu. Alexandrov et al., Nucl. Instr. Meth. A **408**, 359 (1998)
18. S. Paul, PPE 92/199; W. Brückner et al., MPI HV-14 (1995)
19. W. Brückner et al., Nucl. Instr. Meth. A **313**, 345 (1992)
20. W. Brückner et al. , Nucl. Inst. Meth. A **357**, 274 (1995)
21. W. Beusch et al. , Nucl. Instr. Meth. A **323**, 373 (1992); H.-W. Siebert et al. , Nucl. Instr. Meth A **343**, 60 (1994); U. Müller et al., Nucl. Instr. Meth. A **343**, 279 (1994)
22. D. Acosta et al., Nucl. Instr. Meth. A **308**, 481 (1991)
23. M. Beck et al., Nucl. Instr. Meth. A **355**, 351 (1995)
24. W.Heitler, *The Quantum Theory of radiation* (Clarendon Press, Oxford, 1954)
25. GEANT 3.21, CERN Program Library W5103, CERN 1993
26. I. Eschrich (SELEX collaboration), talk presented at BARYONS'98, hep-ex/9811003